Theor Chem Acc (1998) 100:21–30
DOI 10.1007/s002149800m58

Theoretical
Chemistry Accounts

Regular article

Reaction path following by quadratic steepest descent*

Frank Eckert, Hans-Joachim Werner

Institut für Theoretische Chemie, Universität Stuttgart, Pfaffenwaldring 55, D-70569 Stuttgart, Germany

Received: 28 July 1998 / Accepted: 10 August 1998 / Published online: 28 October 1998

Abstract. An efficient steepest descent algorithm for the integration of minimum energy paths, based on local quadratic approximations of the potential energy surface, is presented. The algorithm incorporates a selection procedure for the points at which the second derivatives of the energy are calculated fully or partially, thus minimizing the computational effort while maintaining high accuracy. This makes the method especially well suited for application in variational transition state theory calculations with tunnelling corrections, which have very high accuracy requirements. The performance of the algorithm is illustrated by ab initio calculations for four chemical reactions of differing complexity. The overall computational cost is less than for, or comparable to that of, first- or second-order algorithms published previously.

Key words: Ab initio potential energy surface – Intrinsic reaction coordinate – reaction path following – Quadratic steepest descent

1 Introduction

The pathway of a chemical reaction can be described theoretically by tracing the hypothetical trajectory initiated at the saddle point on the potential energy surface (PES) with all inertia effects removed (i.e. the kinetic energy is neglected throughout). The first definition of such a path was the intrinsic reaction coordinate (IRC) of Fukui [1] in the frame of mass-weighted Cartesian coordinates. However this definition is not unique [2–5], and it is possible to define the reaction path in slightly more general terms as the minimum energy path (MEP) pointing downwards from the saddle point in the direction of steepest descent towards the product and reactant minima of the PES, respectively [2]. A reaction path defined as a MEP on the PES of a polyatomic chemical system is perhaps the most useful and physically meaningful source of information when systems with $N \geq 4$ atoms are studied, since it offers a possibility to overcome the "dimensionality dilemma" of PES with many degrees of freedom [3–8]. The availability of analytic energy gradients and higher derivatives of ab initio PES [9] has made the development of efficient reaction path following methods possible (for reviews, see Refs. [10–16].

The basic problem of reaction path following is the solution of the system of differential equations, Eq. (1), characterized by the coordinate and gradient vectors $\mathbf{x}$ and $\mathbf{g}$ of the PES

$$\frac{d\mathbf{x}(s)}{ds} = -\frac{\mathbf{g}(s)}{|\mathbf{g}(s)|}. \tag{1}$$

The quantity s is the arc length of the reaction path. The simplest solution to Eq. (1) derives from initiating the integration by making one step along the imaginary-frequency normal mode of the Hessian matrix at the transition state geometry of the reaction. Then successive steps along the negative gradients using a small finite step size h are to be taken

$$\mathbf{x}(s+h) = \mathbf{x}(s) - h \cdot \frac{\mathbf{g}(s)}{|\mathbf{g}(s)|}. \tag{2}$$

This first-order integration scheme complies with a linear piecewise approximation of the path of steepest descent and is known as the Euler method for the integration of first-order differential equations [17]. However, due to the fact that the system of differential equations defining a MEP is often "stiff" [14–16] (for the definition of stiffness, see Ref. [17], the Euler steps tend to oscillate around the true MEP. Thus, very small step sizes will be needed to yield a proper MEP. In practice far too many steps – each one requiring an energy and gradient calculation – are needed to achieve acceptable accuracy, making the Euler integration inapplicable for ab initio quantum chemical calculations [14–16], since at this level of theory the number of gradient or higher derivative calculations is the limiting factor regarding

* Dedicated to Prof. Dr. Wilfried Meyer on the occasion of his 60th birthday

Correspondence to: H.-J. Werner

the overall computational cost of MEP integration. This implies the need for the development of special integration schemes adapted to the requirements of ab initio or semiempirical quantum chemical calculations. As shown by Truhlar et al. [14–16], the standard integration algorithms of numerical mathematics, such as Runge-Kutta or predictor-corrector schemes (see Ref. [17]), are usually not applicable to the reaction path problem, since these methods, just like the Euler method, tend to oscillate around the true MEP unless a very small step size is used in the integration.

The integration algorithm should be selected according to the intended use of the computed MEP. One can consider two basic motivations for the calculation of a reaction path. First, the MEP can be used to verify reaction mechanisms and transition states on the PES of chemical reactions. In such applications, the quality of the MEP can usually be low and only a small number of points is necessary to represent the MEP. For the sake of computational efficiency, the number of MEP points to be computed should be as small as possible. This can conveniently be achieved using the ''path relaxation'' technique introduced by Elber and Karplus [18]. A modified version of this method allows the simultaneous optimization of reaction paths and transition states [19]. Path relaxation methods minimize the integral over the energy along the reaction path via an N-point discretization and are very efficient if only a few points (typically five to seven) are used to represent the complete path. An alternative approach is supplied by implicit reaction path integration schemes, which try to correct a simple linear Euler step along the gradient by some a posteriori corrector step(s), using the gradient information at some additional geometries. This ''stabilized'' or ''optimized'' Euler scheme was introduced in 1977 by Ishida et al. [20] and modified and improved by several groups in the following years [21–27]. In particular, the optimized Euler method introduced by Gonzalez and Schlegel (GS) [23, 24] allows large step sizes even for highly curved reaction paths while needing only a few additional gradient calculations per integration step and has found widespread use among computational chemists. Basically, the GS algorithm tries to correct the Euler step by constrained optimization of the $N-1$ dimensional hypersphere perpendicular to the path, which is centred at a pivot point $\mathbf{x}^*$ defined by an Euler step of halved step size. Apart from the initiating step, the GS algorithm uses only energies and gradients of the PES, although it is also possible to include higher derivative information [25, 28].

The second major purpose of reaction path computations is the computation of dynamical properties of chemical reactions (reaction rates, kinetic isotope effects, scattering cross-sections, etc.) via statistical theories, i.e. variational transition state theory (VTST) [4, 6, 7, 29–31] or reaction path Hamiltonian methods [8, 32, 33]. Especially the development of ''direct'' techniques in VTST theory [15, 34] made such computations efficient and easy to handle. Direct VTST methods allow immediate processing of the data conceived pointwise from ab initio calculations, saving the substantial effort of fitting the MEP data to an analytical representation. VTST calculations using semiclassical correction terms for quantum-tunnelling effects typically need 30 or more points along the reaction path [34–36]. In addition to geometries and energies, VTST methods also require the projected vibrational frequencies at the points calculated along the path. This means that the Hessian matrix and the tangent vector of the path (i.e. the gradient) have to be computed at these geometries. VTST calculations demand a tightly converged transition state geometry and a reaction path of high quality, since the accuracy of the projected frequencies depends critically on the quality of the tangent vector and thus on the geometry and gradient of the MEP [14, 16, 28]. As has been pointed out by Baboul and Schlegel [28] an error in the reaction path geometry of 4×10^{-4} a_0 or rad might lead to deviations of over 100 cm^{-1} in the corresponding projected frequencies, becoming even worse if the geometry of the transition state is not optimized punctiliously. In order to reduce the errors in the projected frequencies to 1 cm^{-1} or less, it will be necessary to calculate the geometries of the MEP to an accuracy of 10^{-5} a_0 or rad.

In principle, all of the algorithms mentioned above are suitable for MEP computations in VTST methods if the strict accuracy requirements are met, i.e. if the step size chosen is sufficiently small and if the constrained optimization is converged very tightly [16, 28]. However, Garrett et al. [16] reported that the GS algorithm failed to compute the reaction path with the necessary accuracy if only energies and gradients are used in the constrained optimization. If the Hessian matrix computed along the path is considered in the hypersphere optimization, the accuracy is improved considerably [28]. However, in this case the efficiency of the GS method will be quite low, since apart from the gradient calculation for the Euler step and the Hessian calculation, the constrained hypersphere optimization will require several additional gradient calculations per integration step. Thus, second-order integration schemes [32, 37–41] that use the Hessian matrix explicitly in the integration step and not just in the stabilization step, offer a favourable combination of reaction path integration and calculation of projected frequencies. In the case of VTST calculations optimum computational efficiency in computation of the MEP is reached if the second-order integration algorithm requires only the gradients and Hessian matrices that are also needed in the VTST calculation (i.e. no additional gradient steps), while achieving the required accuracy with a reasonably large step size. Similar implementations of such second-order algorithms based on local quadratic approximations (LQA) to the PES have been developed by several groups [32, 37, 38, 42]. Although these LQA methods have been applied successfully to a number of chemical reactions [38, 43–48], the fact that the step size has to be quite small (around 0.1 a_0 or rad) to achieve the accuracy required in VTST calculations [16, 39] remains unsatisfying. The somewhat more sophisticated algorithm of Sun and Ruedenberg [39–41] was claimed to allow larger step sizes, but so far it has not been tested on ab initio PES of real molecular systems. The proposed second-order quadratic steepest

descent (QSD) algorithm which is introduced in Sect. 2 is based on the algorithm of Sun and Ruedenberg [39–41]. It will be shown that the method is able to meet efficiently both of the demands of MEP computations mentioned above. It is especially well suited for the prospect of VTST calculations.

An important point, relevant to all algorithms that attempt to integrate Eq. (1), is the lack of a local criterion to determine whether a particular point is actually on the "true" MEP. This holds even if the algorithm uses some kind of constrained optimization to converge back to the path [10]. Thus, it is necessary to carefully check the convergence of any new algorithm on different types of PES. In this work, four different chemical reaction systems of varying complexity with 3 to 21 effective degrees of freedom are used to test the proposed algorithm at the ab initio level of theory.

2 Method

The basic formulation of the algorithm has been given in detail by Sun and Ruedenberg [39, 40], and we therefore give only a short summary of the working equations. The potential energy around a given geometry $\mathbf{x}^{(k)}$ is approximated locally by a quadratic Taylor expansion

$$E^{(2)}(\mathbf{x}) = E(\mathbf{x}^{(k)}) + (\mathbf{x}-\mathbf{x}^{(k)})^{\dagger}\mathbf{g} + \tfrac{1}{2}(\mathbf{x}-\mathbf{x}^{(k)})^{\dagger}\,\mathbf{H}(\mathbf{x}-\mathbf{x}^{(k)})\;, \tag{3}$$

where $\mathbf{g}$ and $\mathbf{H}$ are the gradient and Hessian, respectively, at the expansion point $\mathbf{x}^{(k)}$. A MEP as defined by Eq. (1) can be expressed in a computationally convenient manner in terms of a parameter $u(s)$, mapping the arc length of the reaction path between the boundaries $0 \le u \le 1$ [39]

$$u(s) = \exp\alpha\left[\int^{s} |\mathbf{g}[\mathbf{x}(\sigma)]|^{-1} d\sigma\right]\;, \tag{4}$$

where α is an arbitrary constant of dimension $[H/a_0^2]$ which is set equal to unity. Using Eqs. (3) and (4), Eq. (1) becomes

$$\frac{d\mathbf{x}(u)}{du} = u^{-1}\left[\mathbf{g} + \mathbf{H}\cdot(\mathbf{x}-\mathbf{x}^{(k)})\right]\;. \tag{5}$$

Numerical integration of Eq. (5) leads to a piecewise quadratic approximation of the MEP – the local QSD lines $\mathbf{x}(u)$

$$\mathbf{x}(u) = \mathbf{x}^{(k)} - \mathbf{H}^{-1}(\mathbf{I} - u^{\mathbf{H}})\mathbf{g}\;, \tag{6}$$

where $\mathbf{I}$ is the unit matrix and $u^{\mathbf{H}}$ is defined as

$$\left[u^{\mathbf{H}}\right]_{ij} = \sum_{m} U_{im} u^{\lambda_m} U_{jm}\;. \tag{7}$$

The orthogonal matrix $\mathbf{U}$ and the eigenvalues λ_m are obtained from the diagonalization of the Hessian $\left[\mathbf{U}^{\dagger}\mathbf{H}\mathbf{U}\right]_{mn} = \delta_{mn}\lambda_m$.

2.1 The integration step

The energy along the quadratic approximation $E^{(2)}[\mathbf{x}(u)]$ of the MEP decreases with decreasing u [39]. Thus, following the MEP from the transition state towards a minimum is equivalent to stepping along the QSD line $\mathbf{x}(u)$ in the direction of decreasing u with a step size $\le h$. Accordingly, the actual integration step consists of finding a value $u_{\min}$ that fulfills

$$|\mathbf{x}(u_{\min}) - \mathbf{x}^{(k)}| \le h\;. \tag{8}$$

If all eigenvalues of the Hessian matrix are positive, $u_{\min}$ can be chosen to be zero, i.e. Eq. (6) becomes equivalent to a Newton step restricted to step size h. If the Hessian matrix has negative or zero eigenvalues, $\mathbf{x}(u)$ would lead to infinity if a zero value were used for $u_{\min}$. In this case $u_{\min}$ is found from [39]

$$\mathbf{e}^{\dagger}\left[\mathbf{x}(u_{\min}) - \mathbf{x}^{(k)}\right] = h\;, \tag{9}$$

where $\mathbf{e}$ denotes the eigenvector corresponding to the lowest negative eigenvalue λ of the Hessian matrix. Inserting Eq. (9) into Eq. (6) leads to the condition

$$(u_{\min}^{\lambda} - 1)\mathbf{e}^{\dagger}\mathbf{H}^{-1}\mathbf{g} = h \tag{10}$$

from which $u_{\min}$ and subsequently, by virtue of Eq. (6), $\mathbf{x}^{(k+1)} = \mathbf{x}(u_{\min})$ can be determined.

Sun and Ruedenberg have shown that the straightforward implementation of such an LQA step (i.e. at a given geometry $\mathbf{x}^{(k)}$, compute the energy, gradient and Hessian matrix, build the QSD line and step to the new geometry $\mathbf{x}^{(k+1)}$, where the next energy, gradient and Hessian matrix are computed, and so on [32, 37, 38]) has problems in describing strongly curved reaction paths, causing oscillative behaviour and quite large deviations from the exact MEP [39]. In order to achieve a better description of such reaction paths, Sun and Ruedenberg modified this simple scheme and distinguished three species of points: the $\mathbf{x}^{(k)}$ points, where energy, gradient and Hessian matrix are calculated, the $\mathbf{p}^{(k)}$ points, where the quadratic approximations to the MEP are pieced together and finally the $\mathbf{r}^{(k)}$ points, which represent the actual "points on the MEP". Obviously, the most reasonable choice is to place the $\mathbf{p}^{(k)}$ points right between the $\mathbf{x}^{(k)}$ points, since in this case the quadratic Taylor expansion will be about the centre of the QSD line rather than the beginning of the step. Starting from an old connection point $\mathbf{p}^{(k-1)}$ and an expansion centre $\mathbf{x}^{(k)}$, the actual QSD step consists of computing the gradient and the Hessian matrix at $\mathbf{x}^{(k)}$ and constructing the QSD line around this point, starting from the old $\mathbf{p}^{(k-1)}$ point, then stepping h along this line to obtain the next connection point $\mathbf{p}^{(k)}$. The new expansion centre $\mathbf{x}^{(k+1)}$ is then found by stepping another $h/2$ along this line. The corresponding $\mathbf{r}^{(k)}$ point is found by stepping back from $\mathbf{p}^{(k)}$ with a step size of $h/2$ on the actual steepest descent line. The $\mathbf{r}^{(k)}$ point will be near the $\mathbf{x}^{(k)}$ point, but generally much closer to the exact path than $\mathbf{x}^{(k)}$ is. It can be argued that such a QSD step of step size h will achieve the accuracy of a simple step of halved step size $h/2$ [39]. Thus, it should allow much larger step sizes than a simple LQA step. The QSD scheme described above was proposed by Sun and Ruedenberg for use with an exact Hessian matrix in each integration step [39]. They suggested a slightly modified scheme if poorer approximations of Hessian matrix were used [40], However, we found that the scheme described above always achieved the best accuracy in the practical MEP computations, independent of the approximation of the Hessian matrix. Accordingly, this scheme will be used throughout the current work.

2.2 Step adaption

The curvature of the reaction path can be utilised to adjust the step size of the QSD method to yield an optimum description of the actual features of the reaction path. If a strong curvature is present, the step size should be reduced to improve the stability and accuracy of the numerical integration. The curvature vector $\mathbf{k}$ is defined generally as

$$\mathbf{k} = \frac{d\mathbf{t}}{ds} = \frac{d^2\mathbf{x}^{(k)}}{ds^2}, \qquad \text{where} \qquad \mathbf{t} = \mathbf{g}/|\mathbf{g}|\;. \tag{11}$$

The curvature vector of the reaction path [49] is in the frame of the LQA Eq. (3):

$$\mathbf{k} = (\mathbf{I} - \mathbf{t}\mathbf{t}^{\dagger})\mathbf{H}\mathbf{t}/|\mathbf{g}|\;. \tag{12}$$

The step size can be expressed as a function of the scalar curvature k defined as the norm of Eq. (12). Following Sun and Ruedenberg [39, 49], the step size is expressed as the monotonous function Eq. (13):

$$h(k) = h_{\max}\cdot f(k/\tilde{k}) \qquad \text{where} \qquad f(k/\tilde{k}) = a + \frac{1-a}{1+(k/\tilde{k})^{v}}\;. \tag{13}$$

The adjustable parameters were chosen to be $a = 1/4$, $v = 5/6$ and $\tilde{k} = 2.0\; a_0^{-1}$ or rad^{-1}. Using these values, the scaling factors $f(k/\tilde{k})$

observed in the strongly curved regions of the MEP of the test systems were between 0.4 to 0.6 for maximum step sizes of $h_{max} = 0.3$, 0.5 and 0.7 a_0 or rad. Smaller values of $\tilde{k}$, as used in Refs. [39, 40] tend to dampen the step too much, even in regions of moderate to small curvature.

The accuracy of the step adjustment procedure is improved if the tangent vector **t** used in Eq. (12) is defined at the $\mathbf{p}^{(k)}$ points instead of at the $\mathbf{x}^{(k)}$ points. In this case, the gradient vector used to compute **t** should be adjusted to the $\mathbf{p}^{(k)}$ point geometries by $\mathbf{g}(\mathbf{p}^{(k)}) = \mathbf{g}(\mathbf{x}^{(k)}) + \mathbf{H} \cdot (\mathbf{p}^{(k)} - \mathbf{x}^{(k)})$.

2.3 Initiation

The integration of a MEP is normally started at the transition state geometry of the reactive system. Since the gradient is zero at transition state geometries, the first step cannot be determined from Eq. (6). Instead, the first step is taken along the eigenvector of the Hessian matrix that is associated with its negative eigenvalue, i.e. in the direction of the "transition vector". In practice it was convenient to step along the transition vector with the step size h that is also used in the successive QSD steps. In the first QSD step the transition state geometry was used as the first **p** point and the point reached along the transition vector was taken as the first expansion centre. Similarly, the curvature vector at the transition state cannot be determined from Eq. (12). The correct calculation of the curvature would involve third derivatives of the energy [10, 32]. Thus, for efficiency considerations no step adaption was accomplished in the initiation step.

If the integration is initiated at a non-stationary point, a simple LQA step of step size $h/2$ is used to obtain the starting geometries for the first QSD step. The geometry predicted by the LQA step will then be chosen as the first x point, while the starting geometry will be the first **p** point. Using these points, it is possible to continue with a regular QSD step as described in the previous sections. Since the accuracy of the simple LQA step of halved step size is approximately that of the QSD step of step size h [39], the overall accuracy of the path will not be impaired by the initiating step. We found that the complicated initiation procedure proposed in Ref. [39] that includes two additional steps with low step sizes, was not efficient in practice since it did not lead to higher accuracy. The simple initiation scheme used here always yielded sufficient accuracy.

2.4 The Hessian matrix

The approximation of the Hessian matrix is crucial to the accuracy of the QSD method. However, its calculation is also the computationally most demanding part of the reaction path integration. If no analytical second derivatives of the energy are available for a given ab initio wavefunction they have to be approximated by numerical differentiation of gradients calculated at additional points. The Hessian matrix can be obtained either from a least-squares fit procedure, as used in Ref. [40], or from a finite difference scheme [50]. As noted by Pulay [51], for a given number of distorted gradient points, the latter will generally yield better results. Thus, finite differences were used in all test calculations. Our actual implementation of the QSD method allows the use of forward differences or of the more accurate central differences [50], using n or $2n$ additional gradient calculations to recalculate the complete Hessian, where n is the number of degrees of freedom.

Due to high computational cost, the exact analytical or numerical calculation of the Hessian matrix in each optimization step is only feasible for very small systems if ab initio wavefunctions are used. Alternatively, the Hessian can be adjusted along the reaction path by some update procedure that uses the geometries and gradients of previous $\mathbf{x}^{(k)}$ points. If the Hessian possesses only positive eigenvalues, the BFGS algorithm [52] is used. Near the transition state Powell's algorithm [53] or the combined Murtagh-Sargent-Powell (MSP) update of Bofill [54] can be employed. Since in many tests the MSP update showed superior performance, it was used for all calculations in Sect. 3. Depending on the eigenvalue structure of the Hessian and on the norm of the gradient, the QSD algorithm switches between the BFGS and MSP schemes.

Due to the well-known deficiencies of the updating schemes [55–57] it seems reasonable to include some regeneration steps, where the Hessian is recalculated either partly or completely. In the simplest case the complete Hessian is recomputed after each *ireg* integration step. This strategy is especially well-suited for "interpolated VTST" methods [58] that use a reduced number of Hessian calculations along the MEP (e.g. an exact Hessian on each second or third point on the MEP) and interpolate the projected frequencies at the intermediate points. However, this "static" regeneration scheme does not take into account that the Hessian changes much more rapidly in some regions of the MEP than in other parts. The efficiency and accuracy of the QSD step can be increased significantly if the frequency of the regeneration is adjusted to the actual changes of the Hessian matrix along the reaction path. Such "dynamic" regeneration can be achieved by checking the root mean square (RMS) of the changes imposed by the update procedures on all matrix elements of the exact Hessian. Another criterion for dynamic regeneration is the overall relative change of the Hessian elements. In practice the two regeneration criteria behaved very similarly. The main problem of a criterion based upon the difference of an updated Hessian element and an exact one is the quality of the update procedure. If the modification of the Hessian elements imposed by the update is too weak, the dynamic regeneration will be triggered too late or never. This would lead to errors in the QSD step. However, a careful check of all the systems tested in this work showed that the change of the Hessian elements imposed by the update procedures was always too large in comparison to the exactly recalculated values. This was especially true for the Powell update, which often greatly overshoots the exact change. The criteria for the dynamic regeneration remain valid in this case, since the procedure can easily be prevented from regenerating the Hessian too often by adjusting the corresponding threshold value for the RMS or percental change.

If the Hessian is calculated numerically, it is reasonable to regenerate only the elements of the Hessian matrix that actually change significantly along the MEP. The criterion for this "partial" regeneration scheme can be chosen analogously to the dynamic criteria. Regarding efficiency and accuracy, the best performance was achieved by checking the relative change of each individual Hessian element after the update. A combination of the dynamic and the partial criteria (i.e. recalculate only selected elements at dynamically chosen intervals) did not lead to an improvement in the overall efficiency since it was necessary to choose a very tight criterion either for the partial or for the dynamic regeneration to achieve the necessary accuracy. A different partial regeneration scheme was proposed in Ref. [40]: in each integration step one coordinate is distorted by a small amount. The gradient of the resulting geometry is then used in Powell's update formula to correct the Hessian matrix. If all coordinates are distorted successively during the course of the integration, the Hessian will be regenerated gradually. In practice, we found that this regeneration scheme was very inefficient. In comparison with the update using previous MEP geometries only, the additional gradient calculations did not improve the overall accuracy of the QSD step. We believe that this is mainly due to the fact that systematic distortion of all coordinates does not take into account the situation on the reaction path. Accuracy and efficiency will be much higher if only those parts of the Hessian matrix which actually undergo strong changes during integration are regenerated. This presumption was confirmed by the test calculations presented below.

3 Results and discussion

The algorithm outlined in Sect.2 has been implemented in the MOLPRO program package [59]. To illustrate the performance of the method, the reaction paths of four different chemical reactions were calculated at the HF/3-21G level of theory. This method and basis set, which has also been used in previous studies, will clearly not

lead to quantitatively correct results, but is sufficient for the present testing purpose. All pathways were computed in nonredundant internal coordinates, taken from Ref. [60]. The accuracy of the reaction path was regarded as sufficient if deviations from the exact path were below 10^{-5} a_0 or rad for all internal coordinates. The path integrations were initiated at the transition states of the reactions, which were optimized tightly, using a threshold of 10^{-6} a.u. for the RMS of the gradient components. The integration was terminated at the product and reactant minima structures if the standard thresholds of the geometry optimization program of MOLPRO [61] were met. All test calculations were performed with maximum step sizes of 0.15, 0.3, 0.5 and 0.7 a_0 or rad. The Hessian matrices at the transition state and the regeneration points were calculated numerically, using forward differences of analytical gradients. The dynamic regeneration was performed if the RMS deviation of the Hessian elements before and after update was larger than 0.5 a.u. In numerous test calculations this value was found to be the best compromise between accuracy and efficiency. Partial regeneration was performed if the relative deviation of an individual element of the Hessian matrix before and after update $|(H_{ij}^{\text{updated}} - H_{ij})/H_{ij}|$ was larger than 0.1. This threshold has been chosen to be somewhat stricter than the dynamic one since increasing this value leads to rapidly decreasing accuracy of the QSD step. However, when the threshold was even stricter (i.e. 0.05 or below) the accuracy did not increase substantially. This implies the existence of some "critical" threshold for the partial update. To ensure that all important elements of the Hessian are recalculated it is necessary to stay below this threshold.

The "exact" reaction pathways were computed using the QSD method with a step size of $h = 0.05$ a_0 or rad using a completely regenerated Hessian matrix in each integration step. To verify these paths, the GS algorithm [23, 24] as implemented in Gaussian94 [62] was used with the same step size and a convergence threshold of 10^{-6} a.u. for the RMS gradient. The RMS deviations between the exact paths of the two methods were below 10^{-6} a_0. Thus, the QSD path can be regarded as exact in the limit of small step sizes. Note that the following results show the deviations of the $\mathbf{x}^{(k)}$ points from the the exact path. The somewhat less accurate $\mathbf{x}^{(k)}$ points were used in order to achieve an unbiased comparison with other integration algorithms used for VTST computations, since the $\mathbf{x}^{(k)}$ points are also the geometries where the projected frequencies are calculated. When the $\mathbf{r}^{(k)}$ points were used, the deviations from the exact path were typically 1–2 orders of magnitude lower than the values obtained using the $\mathbf{x}^{(k)}$ points.

3.1 HCN → HNC isomerization

Due to its well-known features [63, 64], the isomerization of hydrogen cyanide has frequently been used to test MEP integration algorithms [14, 20, 21, 23, 27]. The results of the QSD reaction path algorithm in terms of the number of points on the MEP, the number of necessary gradient calculations (including numerical Hessian computations) and the resulting accuracies for a variety of step sizes are presented in Table 1. The results of the QSD method for step sizes of $h_{\max} = 0.3(\triangle)$, $0.5(\triangledown)$ and $0.7(+)$ a_0 or rad for the case of a partially regenerated Hessian matrix are depicted in Fig. 1.

As can be expected, using a small step size of 0.15 a_0 and/or frequent regeneration of the Hessian matrix the QSD method yields excellent accuracy. For more typical step sizes of 0.3 a_0 or larger, the errors increase rapidly when increasing *ireg* in the static regeneration scheme (see Table 1). The largest error always occurs at a H-C distance of around 1.2 Å (cf. Fig. 1), a region where the Hessian changes rapidly along the MEP. Obviously, the MSP update cannot modify the Hessian properly in that region. If the Hessian is regenerated exactly in this region, as is achieved by the dynamic procedure, the error is much lower. This explains why dynamic regeneration, while needing exactly the same number of gradient calculations (for example four Hessian regenerations in the case of $h_{\max} = 0.3$ a_0 and $ireg = 7$), yields higher accuracy

Table 1. Integration steps, gradient calculations and largest errors of quadratic steepest descent (QSD) reaction path calculations for the HCN ↔ HNC isomerization[a]

Hessian regeneration	$h_{\max} = 0.15$			$h_{\max} = 0.3$			$h_{\max} = 0.5$			$h_{\max} = 0.7$		
	ns	ng	Δ	ns	ng	Δ	ns	ng	Δ	ns	ng	Δ
Static: *ireg* = 1[b]	56	218	0.1	34	130	0.7	24	90	2.9	18	66	59.0
Static: *ireg* = 3[b]	56	110	0.1	34	64	1.4	24	45	11.7	18	33	189.0
Static: *ireg* = 7[b]	56	77	0.1	34	46	51.1	24	33	280.6	18	24	312.4
Static: *ireg* = ∞[b]	56	56	0.5	34	34	654.6	24	24	690.1	18	18	715.3
Dynamic[c]	56	71	0.1	34	46	2.5	24	39	76.9	18	33	336.5
Partial[d]	56	97	0.1	32	68	1.5	24	61	7.5	18	53	526.3

[a] Coordinate definitions were taken from Ref. [60]. $h_{\max}$: maximum step size in a_0 or rad. ns: number of integration steps. ng: number of gradient calculations. Δ: largest deviation of the QSD points from the exact path, in 10^{-6} a_0 or rad

[b] Static regeneration of the complete Hessian matrix after *ireg* integration steps

[c] Dynamic regeneration of the complete Hessian matrix if the RMS deviation of the updated Hessian matrix from the original one was larger than 0.5 a.u.

[d] Regeneration of selected Hessian matrix elements if the relative deviation of the updated Hessian matrix elements from the original ones was larger than 0.1

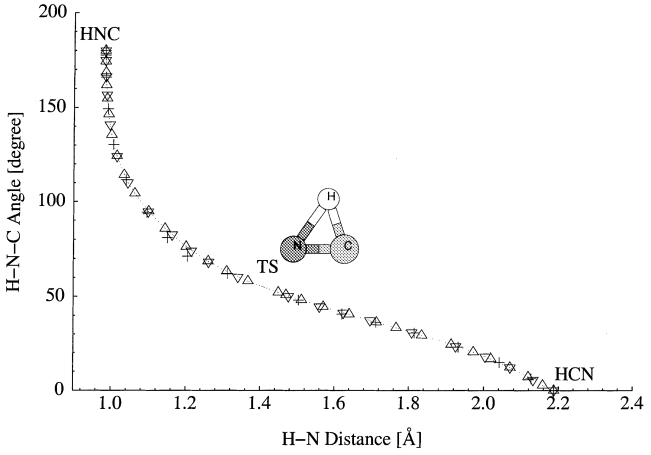

Fig. 1. Quadratic steepest descent (QSD) reaction path of the $HCN \leftrightarrow HNC$ isomerization for step sizes of $h_{max} = 0.3(\triangle), 0.5(\triangledown)$ and $0.7(+)$ a_0 or rad. Selected Hessian elements were recalculated during the integration

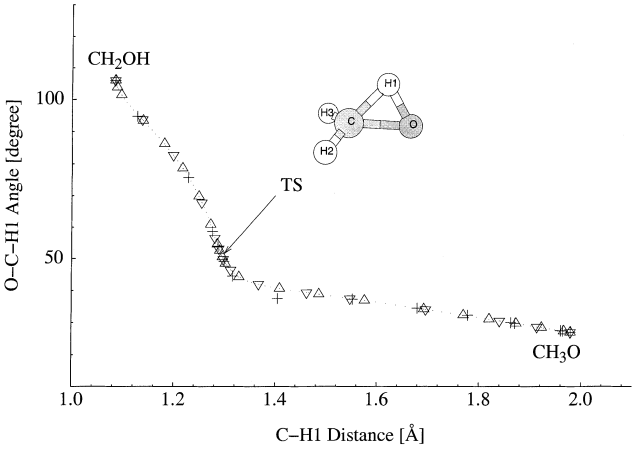

Fig. 2. QSD reaction path of the $CH_3O \rightarrow CH_2OH$ rearrangement for step sizes of $h_{max} = 0.3(\triangle)$, $0.5(\triangledown)$ and $0.7(+)$ a_0 or rad. Selected Hessian elements were recalculated during the integration

than the static procedure (cf. Table 1). The partial regeneration scheme yields even better accuracy, in particular for larger step sizes; however, the total number of gradient calculations is larger in this case. It should be noted that for the smallest step size the accuracy is maintained even without any Hessian regeneration. In any case the minima were always reached safely with all the step sizes tested.

3.2 $CH_3O \rightarrow CH_2OH$ rearrangement

The rearrangement of the methoxy radical to hydroxymethylene provides a test case of higher complexity, since the curvature of the MEP changes strongly from the transition state to the CH_2OH minimum, eventually going through zero at an intermediate bifurcation point of the PES [65, 66]. Moreover, it is difficult to represent the geometry of the system in nonredundant internal coordinates without imposing strong couplings [19]. Using the *Z*-matrix coordinates from Ref. [60], the system of differential equations defining the MEP becomes very stiff in the direction of the CH_2OH minimum. This is mainly due to couplings in the coordinates. Nevertheless, this *Z*-matrix was used in order to obtain a test case with a very stiff MEP.

The performance of the QSD algorithm is presented in Table 2, and the MEP is depicted in Fig. 2 for the partial Hessian regeneration scheme. As can be seen from Table 2, the static regeneration scheme leads to substantial deviations from the exact path if the regeneration frequency is low. The errors are a consequence of strong couplings in the coordinates. It is also clear that the QSD algorithm can deal with the stiffness caused by these couplings if the quality of the Hessian matrix is high, as is the case for frequent regeneration. As in the case of HCN, the problems are caused mainly by the updating procedure. The quality of the Hessian updated by the MSP or Powell scheme is very poor in the direction of the CH_2OH minimum. Moreover, these updating schemes retain the negative eigenvalue of the Hessian matrix far too long. One way to overcome this problem is to modify the threshold for switching between updates in order to obtain an "earlier" BFGS update. However, this seems quite arbitrary and presumes some prior knowledge about the MEP and the projected frequencies. The dynamic regeneration procedure achieves this automatically, since the Hessian is recalculated just at the critical geometries, which leads to much better results with fewer gradient computations. The same is also true for the partial regeneration scheme. At the self-consistent field level, the changes in

Table 2. Integration steps, gradient calculations and largest errors of QSD reaction path calculations for the $CH_3O \rightarrow CH_2OH$ rearrangement[a]

Hessian regeneration	$h_{max} = 0.15$			$h_{max} = 0.3$			$h_{max} = 0.5$			$h_{max} = 0.7$		
	ns	ng	Δ	ns	ng	Δ	ns	ng	Δ	ns	ng	Δ
Static: *ireg* = 1	38	254	0.1	23	149	3.6	15	93	7.5	14	86	256.3
Static: *ireg* = 3	38	110	0.3	23	65	63.1	15	39	308.4	16	40	743.6
Static: *ireg* = 7	38	68	2.4	23	41	81.1	15	27	861.2	19	37	1792.5
Static: *ireg* = ∞	38	38	2.4	23	23	135.5	15	15	1574.8	19	19	3699.2
Dynamic	38	50	2.4	23	35	8.7	15	33	481.0	16	34	784.8
Partial	38	141	0.3	23	90	4.5	15	56	18.0	16	60	379.8

[a] Notation and parameters as in Table 1

the Hessian along the MEP are dominated by three coordinates [65]. This is reflected in the partial regeneration of the Hessian, showing an average of about three additional gradient calculations (cf. Table 2). Under similar conditions (i.e. integration in nonredundant internal coordinates using a step size of 0.3 a_0) the GS algorithm provided 15 points on the reaction path, while needing 57 gradient calculations [19], while the present calculation neeeded 35 gradient calculations with the dynamic update and provided 23 points.

3.3 $CH_3CH_2F \rightarrow CH_2CH_2 + HF$ reaction

The elimination of hydrogen fluoride from ethyl fluoride is a bimolecular reaction with a four-centred ring transition structure. The PES of this reaction has been studied by Kato and Morokuma [67] at the SCF/4-31G level of theory. The reaction path was found to be dominated by the change of five internal coordinates (the intermolecular distance, the angle describing the relative orientation of the H-F fragment, the H-F distance, the C-C distance and the C-C-H angles; see Fig. 3). In the region around the MEP has a large curvature the transition state which decreases rapidly as the reaction proceeds towards the reactant or the product minima of the PES. In addition, the crucial five coordinates are strongly coupled in the *Z*-matrix used to represent the geometry of the system, which was taken from Ref. [60]. These factors make this reaction a tough test case. If a coordinate set with lower couplings were used, the performance of the algorithm could be improved substantially.

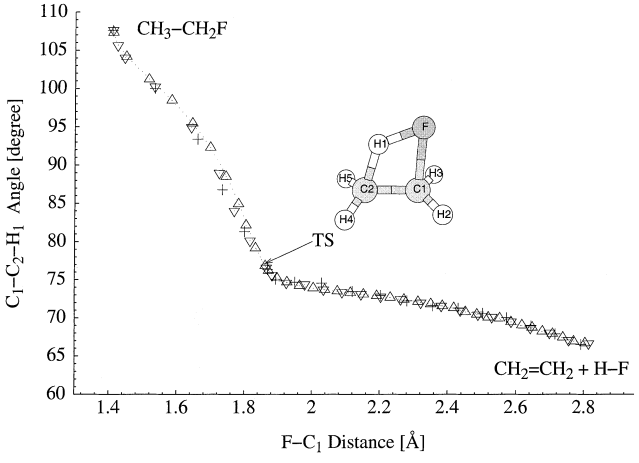

Fig. 3. QSD reaction path of the four-centred elimination reaction $CH_3CH_2F \rightarrow CH_2CH_2 + HF$ for step sizes of $h_{max} = 0.3(\triangle), 0.5(\triangledown)$ and $0.7(+)$ a_0 or rad. Selected Hessian elements were recalculated during the integration

As can be seen from Table 3, the static regeneration scheme shows quite substantial errors even for small step sizes. If the regeneration interval for the Hessian is larger than two, the QSD path shows oscillations near the transition state in the direction of the fragmentation. The relatively small step the QSD method takes in this region (see Fig. 3) is due to the strong curvature. Since the Hessian still has one negative eigenvalue near the transition state, the BFGS update cannot be used in the critical region of the MEP. The MSP update obviously introduces large errors into the Hessian. This clearly confirms the need for a better "transition state update" procedure, allowing a free development of the Hessian eigenvalue structure, as has been pointed out recently by Bofill et al. [54, 56, 57]. However, the dynamic and partial regeneration schemes are able to cope with those problems. Especially, the dynamic procedure was very efficient in this reaction (cf. Table 3). On average, the partial regeneration recomputed around five gradients in each integration step, corresponding to the five leading coordinates reported in Ref. [67].

3.4 Diels-Alder reaction

The parent Diels-Alder reaction of butadiene with ethylene has been the subject of many theoretical studies [68]. The curvature of its MEP is very strong in the product region and around the transition state. This is visible from the reduced effective step size of the QSD method in those regions of the MEP (cf. Fig. 4). Having 21 effective degrees of freedom it is also the largest test system considered here. Regarding the size and complexity of this system it seems slightly surprising that the QSD method achieved the best performance in terms of accuracy and efficiency of all four reactions (see Table 4). For a step size of 0.3 a_0 all regeneration schemes yielded accuracies of the MEP better than 10^{-5} a_0. This was true even if the Hessian was not recalculated at all (i.e. $ireg = \infty$), which indicates that the update of the Hessian matrix works quite well for this system.

Table 3. Integration steps, gradient calculations and largest errors of QSD reaction path calculations for the four-centred elimination reaction $CH_3CH_2F \rightarrow CH_2CH_2 + HF$

Hessian regeneration	$h_{max} = 0.15$			$h_{max} = 0.3$			$h_{max} = 0.5$			$h_{max} = 0.7$		
	ns	ng	Δ	ns	ng	Δ	ns	ng	Δ	ns	ng	Δ
Static: *ireg* = 1	67	782	0.1	43	494	2.5	28	314	35.9	25	278	85.7
Static: *ireg* = 3	67	309	0.5	43	197	19.8	28	127	305.5	25	113	869.2
Static: *ireg* = 7	67	166	10.6	45	111	83.8	31	75	305.5	27	60	869.2
Static: *ireg* = ∞	67	67	43.8	45	45	136.9	35	35	1245.0	27	27	1466.7
Dynamic	67	111	0.5	43	87	8.1	28	72	520.8	25	69	688.9
Partial	67	212	0.3	43	138	5.5	28	128	185.2	25	124	296.2

[a] Notation and parameters as in Table 1

Table 4. Integration steps, gradient calculations and largest errors of QSD reaction path calculations for the Diels-Alder reaction of butadiene and ethene[a]

Hessian regeneration	$h_{max} = 0.15$			$h_{max} = 0.3$			$h_{max} = 0.5$			$h_{max} = 0.7$		
	ns	ng	Δ	ns	ng	Δ	ns	ng	Δ	ns	ng	Δ
Static: *ireg* = 1	55	1168	0.1	30	618	1.5	22	442	3.0	18	354	4.5
Static: *ireg* = 3	55	433	0.1	30	219	1.5	22	169	18.2	18	123	42.5
Static: *ireg* = 7	55	202	0.1	30	114	4.4	22	85	86.4	18	60	154.9
Static: *ireg* = ∞	55	55	0.3	30	30	4.4	22	22	86.4	18	18	154.9
Dynamic	55	55	0.3	30	51	4.4	22	43	27.4	18	39	56.4
Partial	55	210	0.1	30	132	1.5	22	99	3.5	18	92	8.0

[a] Notation and parameters as in Table 1

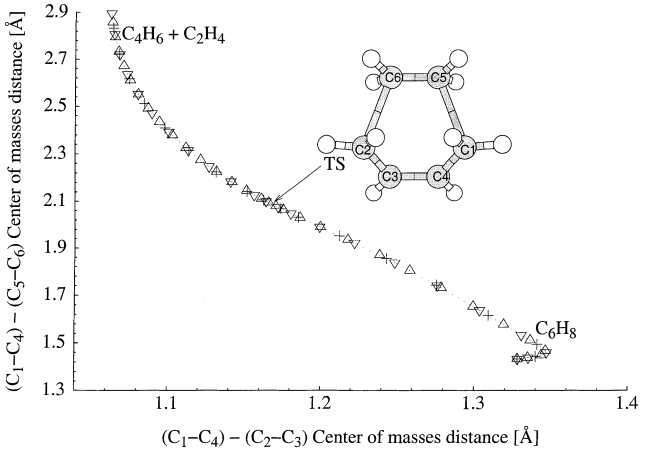

Fig. 4. QSD reaction path of the Diels-Alder reaction of C_4H_6 and C_2H_4 for step sizes of $h_{max} = 0.3(\triangle)$, $0.5(\triangledown)$ and $0.7(+)$ a_0 or rad. Selected Hessian elements were recalculated during the integration

When the Hessian was recalculated in each optimization step, the step size could be increased to 1.2 a_0 without losing the required accuracy, yielding 14 points on the MEP. The partial Hessian regeneration took around three additional gradient calculations per integration step. We found no evidence that the number of relevant Hessian elements increases with the number of degrees of freedom. Using a step size of 0.3 a_0 and comparable conditions, the GS algorithm provided 22 points on the reaction path, while needing 122 gradient calculations [19] compared with 51 gradient calculations for 30 points in the present calculation using dynamic regeneration.

4 Conclusions

We have demonstrated that the QSD algorithm of Sun and Ruedenberg [39] combined with a dynamic or partial Hessian regeneration scheme provides an efficient and reliable way of integrating MEPs on PES of chemical reactions. If molecular dynamics or VTST calculations require second derivatives along the MEP, the QSD algorithm will be more economical than intrinsic "stabilized" or "optimized" Euler schemes, since it does not require any additional gradient calculations at displaced geometries off the MEP for corrective relaxation steps; yet it provides the resulting points on the MEP with high accuracy. The introduction of a dynamic or partial regeneration scheme for the Hessian matrix has been shown to increase the accuracy of the resulting MEP, while simultaneously minimizing the number of necessary Hessian and/or gradient calculations. Moreover, a reasonable selection of points on the MEP is provided, on which the second derivative matrix is computed exactly. For a step size of 0.3 a_0, the dynamic regeneration yielded deviations from the exact path lower than 10^{-5} a_0 or rad in all test reactions. To achieve this accuracy, which meets the requirements of VTST methods, only 1–4 additional Hessian computations along the whole MEP were necessary. In the test systems studied, the partial regeneration scheme computed 2–5 gradients per step to accommodate the Hessian to the actual geometry on the MEP, while the remaining elements were modified using an update procedure. For the test suite of reactions considered, the dynamic regeneration was more efficient than the partial scheme. However, if the number of degrees of freedom of the reaction becomes larger, this ratio is likely to be reversed. We do not expect the effort of the partial regeneration scheme to increase substantially for larger molecular systems, since the number of force constants that change strongly along the path will be low, while changes in most of the remaining Hessian elements are negligible or small. This makes the efficiency of the QSD method comparable to that of the GS method, which typically needs 3–5 additional gradient calculations per integration step for similar accuracy [23, 38]. In addition, the QSD method yields more points on the MEP for a given step size while also providing the projected frequencies at some points of the MEP, which is not the case for the GS method. Due to the possibility of using large step sizes of up to 0.7 a_0 or rad while retaining reasonable accuracy, the QSD algorithm with partial Hessian regeneration is also applicable for verifying transition states and reaction mechanisms. If accuracy requirements are low, it is also possible to use the QSD method without Hessian regeneration. The reactant and product minima of the tested PES were always reached safely. In this case the number of gradient calculations will be exactly the number of points calculated on the MEP.

Acknowledgements. The authors thank the Fonds der Chemischen Chemie for generous support.

References

1. Fukui K (1970) J Phys Chem 74: 4161
2. (a) Marcus RA (1968) J Chem Phys 45: 49; (b) Truhlar DG, Kuppermann A (1971) J Am Chem Soc 93: 1840; (c) McIver JW, Komornicki A (1972) J Am Chem Soc 94: 2625; (d) Pechukas P (1976) J Chem Phys 64: 1516; (e) Mezey PG Theor Chim Acta 54: 95; (f) Fukui K (1981) Acc Chem Res 14: 363; (g) Heidrich D, Quapp W (1984) Theor Chim Acta 66: 245; (h) Quapp W (1995) The invariance of the reaction path description in any coordinate system. In: Heidrich D (ed) The reaction path in chemistry. Kluwer, Dordrecht, pp 95–107
3. Friedrich K, Herman Z, Zahradnik R, Havlas Z (1988) Adv Quantum Chem 19: 247
4. Truhlar DG, Gordon MS (1990) Science 249: 491
5. Chuang Y-Y, Truhlar DG (1998) J Phys Chem 102: 242
6. Truhlar DG, Garrett BC, Klippenstein SJ (1996) J Phys Chem 100: 12771
7. Isaacson AD (1995) In: Heidrich D (ed) The reaction path in chemistry. Kluwer, Dordrecht, pp 191–228
8. Miller WH, Handy NC, Adams JE (1980) J Chem Phys 72: 99
9. (a) Pulay P (1987) Adv Chem Phys 69: 241; (b) Pulay P (1997) In: Schaefer HF III (ed) Modern theoretical chemistry, vol 4. Plenum, New York, p 153; (c) Yamaguchi Y, Osamura Y, Goddard JD, Schaefer HF III (1994) A new dimension to quantum chemistry – analytic derivative methods in ab initio Molecular electronic structure theory. Oxford University Press, Oxford; (d) Helgaker T, Jørgensen P (1988) Adv Quantum Chem 20: 1; (e) Jørgensen P, Simons J (1981) Geometrical derivatives of energy surfaces and molecular properties. Reidel, Dordrecht
10. McKee ML, Page M (1993) In: Lipkowitz KB, Boyd DB (eds) Reviews in computational chemistry vol 4. VCH, New York, p 35
11. Collins MA (1996) Adv Chem Phys 93: 389
12. Schlegel HB (1994) In: Yarkony DR (ed) Modern electronic structure theory. World Scientific P, Singapore, p 459
13. Dunning TH, Kraka E, Eades RA (1987) Faraday Discuss Chem Soc 84: 1476
14. Garrett BC, Redmon MJ, Steckler R, Truhlar DG, Baldridge KK, Bartoll D, Schmidt MW, Gordon MS (1988) J Phys Chem 92: 1476
15. Baldridge KK, Gordon MS, Steckler R, Truhlar DG (1989) J Phys Chem 93: 5107
16. Melissas VS, Truhlar DG, Garrett BC (1992) J Chem Phys 96: 5785
17. (a) Hairer E, Nørsett S, Wanner G, (1993) Solving ordinary differential equations. Springer Berlin Heidelberg New York; (b) Lambert JD (1991) Numerical methods for ordinary differential systems. Wiley New York; (c) Dormand JR (1993) Numerical methods for differential equations. CRC Press, Boca Raton; (d) Celia MA, Gray WG (1992) Numerical methods for differential equations. Prentice Hall, Englewood Cliffs; (e) Fatunla SO (1988) Numerical methods for initial value problems in ordinary differential equations. Academic Press, New York; (f) Shampine LF (1994) Numerical solution of ordinary differential equations. Chapman and Hall, New York
18. (a) Elber R, Karplus M (1987) Chem Phys Lett 139: 375; (b) Jaisen PG, Shepard R (1988) Int J Quantum Chem Symp 22: 183; (c) Czerminski R, Elber R (1990) J Quantum Chem Symp 24: 167; (d) Czerminski R, Elber R (1990) J Chem Phys 92: 5580; (e) Choi C, Elber R (1991) J Phys Chem 94: 751; (f) Fischer S, Karplus M (1992) Chem Phys Lett 194: 252; (g) Sacho LL, Bán MI (1992) Theor Chim Acta 83: 433; (h) Chiu SS-L, McDouall JJW, Hillier IH (1994) J Chem Soc Faraday Trans 90: 1575; (i) Olender R, Elber R (1997) J Mol Struct 398: 63
19. Ayala PY, Schlegel HB (1997) J Chem Phys 107: 375
20. Ishida K, Morokuma K, Komornicki A (1977) J Chem Phys 66: 2153
21. Müller C, Brown LD (1979) Theor Chim Acta 53: 75
22. Schmidt MW, Gordon MS, Dupuis M (1985) J Am Chem Soc 107: 2585
23. Gonzalez C, Schlegel HB (1989) J Chem Phys 90: 2154
24. Gonzalez C, Schlegel HB (1990) J Phys Chem 94: 5523
25. Gonzalez C, Schlegel HB (1991) J Chem Phys 95: 5853
26. Celani P, Robb MA, Garavelli M, Bernardi F, Olivucci M (1995) Chem Phys Lett 243: 1
27. Anglada JM, Bofill JM (1997) Chem Phys Lett 269: 469
28. Baboul AG, Schlegel HB (1997) J Chem Phys 107: 9413
29. Truhlar DG, Isaacson AD, Garrett BC (1985) In: Baer M (ed) The theory of chemical reaction dynamics, vol 4. CRC Press, Boca Raton, p 65
30. Truhlar DG, (1994) J Chem Soc Faraday Trans 90: 1740
31. Duncan WT, Bell RL, Truong TN (1988) J Comput Chem 19: 1039
32. Page M, McIver JW (1988) J Chem Phys 88: 922
33. Walet NR, Klein A, Dang GD (1989) J Chem Phys 91: 2848
34. Truhlar DG (1995) In: Heidrich D (ed) The reaction path in chemistry. Kluwer, Dordrecht, pp 229–256
35. Truong TN, Duncan W (1994) J Chem Phys 101: 7408
36. Bell RL, Tavaeras DL, Truong TN, Simons J (1997) Int J Quantum Chem 63: 861
37. McKelvey JM, Hamilton JF (1984) J Chem Phys 80: 579
38. Ischtwan J, Collins MA (1988) J Chem Phys 89: 2881
39. Sun JQ, Ruedenberg K (1993) J Chem Phys 99: 5257
40. Sun JQ, Ruedenberg K (1993) J Chem Phys 99: 5269
41. Ruedenberg K, Sun JQ (1994) J Chem Phys 100: 6101
42. Page M, Doubleday C, McIver JW (1990) J Chem Phys 93: 5634
43. Doubleday C, McIver JW, Page M (1988) J Phys Chem 92: 4367
44. Koseki S, Gordon MS (1989) J Phys Chem 93: 118
45. Page M, Lin MC, He Y, Choudhury TK (1989) J Phys Chem 93: 4404
46. Caldwell NJ, Rice JK, Nelson HH, Adams GF, Page M (1990) J Chem Phys 93: 479
47. Garrett BC, Koszykowski ML, Melius CF, Page M (1990) J Phys Chem 94: 7096
48. Soto MR, Page M, McKee ML (1991) Chem Phys 153: 415
49. Sun JQ, Ruedenberg K (1993) J Chem Phys 98: 9707
50. Abramovitz M, Stegun IA (1965) Handbood of mathematical functions. Dover, New York
51. Fogarasi G, Pulay P (1985) In: Durig JR (ed) Vibrational spectra and structure, vol 14. Elsevier, Amsterdam, p 125
52. (a) Broyden CG (1970) J Inst Math Its Appl 6: 76; (b) Fletcher R (1970) Comput J 13: 317; (c) Goldfarb D (1970) Math Comput 24: 23; (d) Shanno DF (1970) Math Comput 24: 647
53. Powell MJD (1971) Math Prog 1: 26
54. Bofill JM (1994) J Comput Chem 15: 1
55. Bofill JM, Comajuan M (1995) J Comput Chem 16: 1326
56. Bofill JM (1996) Chem Phys Lett 260: 359
57. Anglada JM, Bofill JM (1998) J Comput Chem 19: 349
58. Corchado JC, Coitino EL, Chuang Y-Y, Fast PL, Truhlar DG (1988) J Phys Chem 102: 2424
59. Werner H-J, Knowles PJ, with contributions from Amos RD, Berning A, Cooper DL, Deegan MJO, Dobbyn AJ, Eckert F, Hampel C, Leininger T, Lindh R, Lloyd AW, Meyer W, Mura ME, Nicklass A, Palmieri P, Peterson K, Pitzer R, Pulay P, Rauhut G, Schütz M, Stoll H, Stone AJ, Thorsteinsson T (1998) MOLPRO (a package of ab initio programs) version 97.5. University of Birmingham, UK (see http://www.tc.bham.ac.uk/molpro/)
60. Baker J, Chan F (1996) J Comput Chem 17: 888
61. Eckert F, Pulay P, Werner H-J (1997) J Comput Chem 18: 1473
62. Frisch MJ, Trucks GW, Schlegel HB, Gill PMW, Johnson BG, Robb MA, Cheeseman JR, Keith T, Petersson GA, Montgomery JA, Raghavachari K, Al- Laham MA, Zakrzewski VG, Ortiz JV, Foresman JB, Cioslowski J, Stefanov BB, Nanayakkara A, Challacombe M, Peng CY, Ayala PY, Chen W, Wong MW, Andres JL, Replogle ES, Gomperts R, Martin RL,

Fox DJ, Binkley JS, Defrees DJ, Baker J, Stewart JP, Head-Gordon M, Gonzalez C, Pople JA (1995) Gaussian 94, revision D.1. Gaussian, Pittsburgh, Pa
63. Pearson PK, Schaefer HF III, Wahlgren U (1977) J Chem Phys 62: 350
64. Peric M, Mladenovic M, Peyerimhoff S, Buenker RJ (1983) Chem Phys 82: 317
65. Colwell SM (1984) Mol Phys 51: 1217
66. Baker J, Gill PMW (1988) J Comput Chem 9: 465
67. Kato S, Morokuma K (1980) J Chem Phys 73: 3900
68. Bernardi F, Bottoni A, Field MJ, Guest MF, Hillier IH, Robb MA, Venturini A (1988) J Am Chem Soc 110: 3050 and references therein